J Mol Model (2013) 19:2657–2668
DOI 10.1007/s00894-013-1809-9

ORIGINAL PAPER

Electronic structure and properties of neutral, anionic and cationic silicon–nitrogen nanoclusters

Muneerah M. Al Mogren · Adel A. El-Azhary · Wad. Z. Alkiali · Majdi Hochlaf

Received: 14 November 2012 / Accepted: 18 February 2013 / Published online: 26 March 2013

Abstract We performed a G3 investigation of the possible stable structures of silicon–nitrogen Si_nN_m clusters where m=1–4, n=1–4, $m+n$=2–5. We considered the neutral, anionic and cationic molecular species in the singlet, doublet and triplet states, as appropriate. For neutral clusters, our data confirm previous DFT and post Hartree-Fock findings. For charged clusters, our results represent predictions. Several molecular properties related to the experimental data, such as the electronic energy, equilibrium geometry, binding energy (BE), HOMO–LUMO gap (HLG), and spin contamination $\langle S^2 \rangle$ were computed. We also derived the vertical electron attachment (VEA), the adiabatic electron affinity (AEA), and the vertical ionization energy (VIE), of the neutral clusters. Similar to their carbon–nitrogen counterparts, the lowest energy structures for neutral and cationic silicon–nitrogen clusters are found to be linear or quasilinear. In contrast, anionic silicon–nitrogen clusters tend to form 3D structures as the size of the cluster increases.

Keywords G3 calculation · Silicon-nitrogen cluster · Spectroscopic and thermochemical properties

Electronic supplementary material The online version of this article (doi:10.1007/s00894-013-1809-9) contains supplementary material, which is available to authorized users.

M. M. Al Mogren · A. A. El-Azhary (✉) · W. Z. Alkiali
Chemistry Department, Faculty of Science, King Saud University, PO Box 2455, Riyadh 11451, Kingdom of Saudi Arabia
e-mail: azhary60@hotmail.com

M. Hochlaf (✉)
Université Paris-Est, Laboratoire Modelisation et Simulation Multi Echelle, MSME UMR 8208 CNRS,
5 bd Descartes, 77454 Marne-la-Vallée, France
e-mail: hochlaf@univ-mlv.fr

Introduction

Nanoclusters represent the middle ground between small gas phase molecular species and the bulk state. Their properties and therefore their possible applications differ greatly dependent on cluster size, and tend to reflect those of the bulk state when the size of the cluster becomes large. A recent important research domain consists of understanding and predicting cluster evolution, and such understanding is mandatory for the application of this class of compounds in chemistry, physics and nanotechnology. Recently, we investigated carbon–nitrogen C_nN_m clusters [1]. The present theoretical work treats their silicon–nitrogen counterparts, Si_nN_m.

Interest in the study of Si_nN_m clusters has increased in recent decades because of their importance in various domains, e.g., astrophysics, atmospheric chemistry, material science, electronics, combustion and plasma physics. Indeed, silicon has been identified in astrophysical media either embedded in grains or in gas phase. This field has garnered further interest since the detection by Turner [2, 3] in 1992 of SiN in the outer circumstellar envelope of the carbon-rich star IRC +10216. In addition, silicon atoms and ions play crucial roles in the chemistry of the low Earth atmosphere [4–8] and of the ionosphere [9]. Silicon-nitride-containing materials possess specific thermal and elasticity properties. They are a popular insulating layer in silicon-based electronics and silicon nitride cantilevers [10–13], and are also used for the sensing parts of atomic force microscopes. Additionally, they are used in the formation of polysilane materials [14], which have non-linear optics properties. Finally, the gas-phase ion-molecule reactions of Si^+ with ammonia and small amines, or reactions of ammonia on Si surfaces or Si clusters, are possible pathways toward a wide variety of $Si_xH_yN_z$ compounds used in catalysis [15–19]. For instance, $Si_xH_yN_z$ compounds are used as effective reagents to convert the reactive and toxic NO into the benign gas N_2 in several NO-

producing combustion systems [20]. Consequently, $Si_xH_yN_z$ species have attracted a relatively large amount of attention both theoretically and experimentally, with several molecular species of this series having been identified in the gas phase and in cooled matrices by means of various experimental and theoretical techniques (see [21–23] for more details).

The SiN molecule has been investigated experimentally by Elhanine et al. [24], Ito et al. [25] and Naulin et al. [26] and by theoretical ab initio methods by Bruna et al. [27] Chong [28] Cai et al. [29], Borin [30] and Jursic [31]. These latter authors deduced a set of spectroscopic parameters for this important astrophysical molecule using the quadratic complete basis set (CBSQ), configuration interaction ab initio computational methods and several hybrid density functional theory (DFT) methods (e.g., B3LYP, B3P86, and B3PW91). Later, Kerkines and Mavridis [32] used state-of-the-art ab initio methodology to study the SiN and SiN^- ground and electronic excited states. They provided accurate values for the electron affinity of SiN and for the SiN and SiN^- spectroscopic constants that compare well with the respective available experimental data (see [32, 33] and references therein).

The triatomic SiN_2, trapped in cooled rare gas matrices, was identified experimentally by Lembke et al. [34] through electron spin resonance (ESR) studies. Si_2N was first presented in a neutralization–reionization mass spectrometric study by Iraqi et al. [35]. Both identifications were later confirmed by means of ab initio and DFT computations [36–44]. Nevertheless, the exact equilibrium geometries of their ground states, i.e., whether linear or cyclic, remained unclear.

In 1994, neutral, anionic, and cationic Si_3N clusters were identified experimentally for the first time by Goldberg et al. [44] using collisional-activation and neutralization-reionization mass spectrometry. These authors also calculated the geometries and harmonic vibrational frequencies of the Si_nN (n=1–3) for the neutral, anionic, and cationic species with polarized split-valence basis sets (6-311+G*) at the Hartree-Fock (HF) and MP2 levels.

Large Si_nN_m ($n+m$=20) clusters were treated using tight-binding and first-principles DFT in either the local spin density approximation (LDA) or the generalized gradient approximation (GGA) by Jackson et al. [45] who showed a tendency for cage formation when $n+m$ is large enough. In 2000, these authors performed structural studies of neutral Si_nN_m clusters ($n+m\leq6$) using similar methodologies [46]. For Si_2N_2 and Si_3N_2 clusters, it is worth citing the detailed HF and post-HF computations of Ornellas and Iwata on Si_2N_2 [47] and of Ueno and Ornellas [48] on Si_3N_2 clusters. Very recently, a mixed $Si_{n-1}N$ (n=1–19) series was investigated by Li et al. [49] using the full-potential linear-muffin-tin-orbital molecular-dynamics (FP-LMTO-MD) method.

The present theoretical work was motivated by the lack of up-to-date theoretical treatments on the Si_nN_m clusters since previous works have consist mainly of theoretical investigations using DFTs prior to 2000, especially for large-sized clusters. In addition, these previous works considered mostly neutral species and very little information is available on the corresponding anionic and cationic species. Here, we performed a systematic study, at the G3 level of theory, of the possible structures of the Si_nN_m (m=1–4, n=1–4, $m+n$=2–5) clusters in the neutral, anion and cation forms in the singlet, doublet and triplet states, as appropriate. As discussed in [1], G3 computations are viewed to provide accurate enough data. Since all isomeric species were obtained at the same level of theory, we established their relative stabilities. Then, we calculated the binding energy (BE), HUMO–LUMO gap (HLG) and $\langle S^2 \rangle$ for the neutral, anion and cation cluster. We deduced also the vertical electron attachment (VEA), the adiabatic electron affinity (AEA), and the vertical ionization energy (VIE) for the neutral clusters at the MP2/6-31G* level of theory. To the best of our knowledge, our work represents the most detailed and complete calculations to be reported for these clusters. The relation between the stability and properties of the predicted clusters is discussed.

Computational details

All computations were done using the G09 suite of programs [50]. Computations were performed for the Si_mN_n, m=1–4, n=1–4 and $m+n$=2–5, clusters, namely the SiN, Si_2N, SiN_2, Si_3N, Si_2N_2, SiN_3, Si_4N, Si_3N_2, Si_2N_3, and SiN_4 clusters, in neutral, anion and cation forms in the singlet, doublet and triplet states, as appropriate, assuming proposed initial structures of these clusters as depicted in Fig. S1. These proposed initial structures were generated intuitively. Computations were done first at the HF/STO-3 G level. The obtained geometries of these structures were further geometry optimized at the HF/6-31G* level and structures with imaginary vibrational frequencies were excluded. Further computations were performed for all predicted structures at the G3 level. For the equilibrium molecular structure optimizations, we used the standard options as implemented in the GAUSSIAN code.

The BE per atom for the neutral cluster was calculated using the Eq.

$$\mathrm{BE} = [\mathrm{mE(Si)} + \mathrm{nE(N)}] - [\mathrm{E(Si_mN_n)}]$$

where nE (Si) and mE (N) are the energies of the isolated C and Si atoms and E (Si_mN_n) is the energy of the neutral cluster at its optimized geometry. For the anionic cluster, the BE per atom was calculated using the Eq.

$$\mathrm{BE} = \left\{[E(\mathrm{Si}^-) + (m-1)E(\mathrm{Si}) + nE(\mathrm{N})] - \left[E\left(\mathrm{Si_mN_n^-}\right)\right]\right\} /(\mathrm{m}+\mathrm{n})$$

where $E\left(Si_mN_n^-\right)$ is the energy of the anionic cluster at its optimized geometry. Similarly, the BE per atom for the cationic cluster was calculated using the Eq.

$$BE = \left\{[E(Si^+) + (m-1)E(Si) + nE(N)] - \left[E\left(Si_mN_n^+\right)\right]\right\} /(m+n)$$

where $E\left(Si_mN_n^+\right)$ is the energy of the cationic cluster at its optimized geometry.

The VEA was calculated using the Eq.

$$VEA = E_{m+n}(eq) - E_{m+n}^-$$

where E_{m+n} (eq) is the energy of the neutral cluster at its optimized geometry and E_{m+n}^- is the energy of the anionic cluster at the corresponding neutral cluster optimized geometry. The AEA, was calculated using the Eq.

$$AEA = E_{m+n}(eq) - E_{m+n}^-(eq) + ZPEC$$

where E_{m+n} (eq) is defined as above and $E_{m+n}^-(eq)$ is the energy of the anionic cluster at its optimized geometry. ZPEC stands for the zero point vibrational energy correction. The value of ZPEC was used without any scaling. The VIE was calculated using the Eq.

$$VIE = E_{m+n}^+ - E_{m+n}(eq)$$

where E_{m+n}^+ is the energy of the cationic cluster at the corresponding neutral cluster optimized geometry.

A detailed description of the G3 method can be found in Refs. [51, 52]. Briefly, the G3 method starts with calculation of an initial geometry at the HF/6-31G* level and a more accurate geometry at the MP2(full)/6-31G* level. The MP4/6-31G*, MP4/6-31+G*, MP4/6-31G (2df,p) and QCISD(T)/6-31G* energies are computed. The first calculation, MP4/6-31G*, is termed E^{base} and refers to the base energy. The difference between the first and second calculation is referred to as ΔE^+ and represents the correction for the diffuse functions. The difference between the first and third calculation is referred to as ΔE^{2df} and represents the correction for the polarization functions. The difference between the first and fourth calculation is referred to as ΔE^{QCI} and represents a correction for the polarization effects beyond the fourth order. Finally, the energy is calculated at the MP2(full)/GTLarge level, where GTLarge refers to a basis set that includes some core and valence polarization functions. ΔE^{G3L} is calculated using the Eq.

$$\Delta E^{G3L} = MP2(full)/G3Large - MP2/6\text{-}31G(2df,p) - MP2/6\text{-}31+G* + MP2/6\text{-}31G*$$

To correct for the higher-level correction (HLC), the correlation energy is calculated between spin-paired electrons using the Eq.

$$\Delta E^{HLC} = -0.00638n_\alpha - 0.002977\left(n_\alpha - n_\beta\right)$$

where n_α and n_β are the number of α and β electrons, respectively. The G3 energy, E^{G3}, is then given by

$$E^{G3} = E^{base} + \Delta E^+ + \Delta E^{2df} + \Delta E^{QCI} + \Delta E^{G3L} + \Delta E^{HLC} + \Delta E^{ZPE}$$

where E^{ZPE} is the zero point energy calculated at the HF/6-31G* level after being scaled by 0.8929.

Results and discussion

For better clarity of the manuscript, the full set of results is given as Supplementary Material. Only those results relevant for the discussion are detailed below. Figure S1 depicts the initial structures of the two-, three-, four- and five-atom systems. The symmetry, term symbol, BE, HLG, spin contamination $\langle S^2 \rangle$, VEA, AEA and VIE of the ground state predicted structure of the SiN, Si_2N, SiN_2, Si_3N, Si_2N_2, SiN_3, Si_4N, Si_3N_2, Si_2N_3, SiN_4 neutral clusters are listed in Table 1. Tables 2 and 3 list the symmetry, term symbol, BE, HLG and $\langle S^2 \rangle$ of the same clusters in the anion and cation forms, respectively. The calculated vibrational frequencies at the HF/6-31+G* level of the G3 method of the predicted ground state clusters are listed in Table 4. The ground state structures of these predicted clusters in the neutral, anion and cation forms are depicted in Figs. 1, 2, 3, 4, 5, 6, 7, 8, 9 and 10, respectively. The symmetry, term symbol, HF/6-31G*, MP2(full)/6-31G* and G3 (0 K) relative energies, BE, HLG, $\langle S^2 \rangle$, VEA, AEA and VIE of all predicated structures of the SiN, Si_2N, SiN_2, Si_3N, Si_2N_2, SiN_3, Si_4N, Si_3N_2, Si_2N_3 and SiN_4 neutral, anion and cation clusters, as appropriate, are listed in Tables S1–S22. Each predicted conformation is given a number, typed in bold face, according to its G3 energy. The structure of all predicted clusters is shown in Figs. S2–S29. In the following, we discuss the structure of each of the considered SiN, Si_2N, SiN_2, Si_3N, Si_2N_2, SiN_3, Si_4N, Si_3N_2, Si_2N_3 and SiN_4 clusters separately. In this discussion, we compare our data for Si_nN_m clusters to their C_nN_m counterparts [1].

Equilibrium structures

SiN

There is only one possible structure of this diatomic cluster, which is linear. This ground state of this neutral cluster is of $^2\Sigma^+$ nature. The calculated relative energies in Table S1 show that the singlet state ($X^1\Sigma^+$) of the SiN anion cluster

Table 1 Binding energy (BE, eV), HOMO–LUMO gap (HLG, eV), spin contamination $\langle S^2 \rangle$, vertical electron attachment (VEA, eV), adiabatic electron affinity (AEA, eV) and vertical ionization energy (VIE, eV) of the neutral clusters. *Sym* Symmetry, *TS* term symbol

[a]HLG and $\langle S^2 \rangle$ are calculated at the G3 level and VEA, AEA and VIE are calculated at the MP2/6-31G* level. The spin contamination $\langle S^2 \rangle$ was calculated at the MP2(full)/GTLarge, see text

Cluster	Sym	TS	BE	HLG[a]	$\langle S^2 \rangle$[a]	VEA[a]	AEA[a]	VIE[a]
SiN	$C_{\infty v}$	$^2\Sigma^+$	3.99	10.6	1.07	2.99	3.18	11.03
Si_2N	$D_{\infty h}$	$^2\Pi_g$	4.35	6.57	0.94	−0.01	0.57	5.54
SiN_2	C_{2v}	$^1A_1$	5.29	9.08		−1.55	0.54	8.31
Si_3N	C_s	$^2A''$	4.57	6.80	0.81	0.93	−0.03	6.12
Si_2N_2	$D_{\infty h}$	$^1\Sigma_g^+$	5.23	8.67		−0.96	0.65	8.39
SiN_3	C_s	$^2A'$	5.46	9.42	0.83	−2.65	0.68	8.99
Si_4N	C_{2v}	$^2B_2$	4.39	6.45	0.79	1.22	3.06	6.02
Si_3N_2	$C_{\infty v}$	$^1\Sigma$	5.73	3.27		7.98	11.10	3.13
Si_2N_3	C_s	$^2A''$	5.13	0.98		0.94	3.15	6.15
SiN_4	C_s	$^1A'$	5.71	9.63		−1.39	−1.11	9.69

is more stable than the triplet state, while for the SiN cation cluster the triplet state ($X^3\Sigma^-$) is more stable than the singlet state. At the G3 level, the singlet state of the SiN anion cluster is more stable than the triplet state by 3.14 eV, while for the SiN cation cluster the triplet state is more stable than the singlet state by 0.69 eV. Although the three levels considered in this work—HF/6-31G*, MP2/6-31G* and G3—have the same energy order for the two predicted structures of the SiN anion and cation clusters, the relative energies of the three levels is different. For example, for the SiN cation cluster at the HF/6-31G*, MP2/6-31G* and G3 levels, the triplet state is more stable than the singlet state by 3.96, 1.68 and 0.69 eV, respectively. Our findings are in good agreement with those of previous investigations [44, 46]. For the corresponding CN clusters, the singlet state was more stable than the triplet state for both the anion and cation clusters.

There is elongation of the SiN bond length of the SiN cluster by either the addition or removal of an electron. At the MP2/6-31G* level, the SiN bond length of the SiN anion cluster is calculated to be about 0.10 Å longer than that of the neutral SiN cluster while that of the SiN cation cluster is calculated to be about 0.25 Å longer than that of the neutral SiN cluster. For the corresponding CN clusters, the CN bond length of the CN anion cluster is calculated to be about 0.06 Å longer than that of the neutral cluster and that of the CN cation cluster is calculated to be about 0.1 Å longer than that of the neutral CN cluster. Notice also that the CN bond lengths of the CN clusters are calculated at the MP2/6-311+G** level while those for the SiN clusters are calculated at the MP2/6-31G* level. Therefore, we redid the computations for the SiN neutral, anion and cation clusters at the MP2/6-311+G* level. The calculated SiN bond length of the SiN neutral, anion singlet and cation triplet clusters are 1.533, 1.633 and 1.781 Å, respectively. These values are too close to those obtained at the MP2/6-31G* level, i.e., within less than 0.01 Å. For the neutral SiN cluster, our value is slightly shorter than that computed previously and measured experimentally [32, 46, 53]. For the SiN equilibrium distance of the SiN anion cluster, the differences between our value, that deduced from the large computations

Table 2 BE (eV), HLG (eV) and spin contamination $\langle S^2 \rangle$ of the anion clusters[a]

Cluster	Sym.	TS	BE	HLG	$\langle S^2 \rangle$
SiN	$C_{\infty v}$	$^1\Sigma^+$	4.91	8.23	
Si_2N	C_{2v}	$^1A_1$	4.73	6.32	
SiN_2	$C_{\infty v}$	$^2\Pi$	5.34	5.69	0.89
Si_3N	C_{2v}	$^1A_1$	4.39	7.34	
Si_2N_2	C_{2v}	$^2A_1$	5.46	7.99	0.81
SiN_3	C_{3v}	$^1A_1$	5.41	8.70	
Si_4N	C_{3v}	$^1A_1$	4.86	7.36	
Si_3N_2	C_{2v}	$^2B_2$	5.37	6.72	0.82
Si_2N_3	C_{2v}	$^1A_1$	5.66	6.90	
SiN_4	C_{2v}	$^2B_2$	5.47	7.65	0.81

[a] See footnote in Table 1

Table 3 BE (eV), HLG (eV) and spin contamination $\langle S^2 \rangle$ of the cation clusters[a]

Cluster	Sym.	TS	BE	HLG	$\langle S^2 \rangle$
SiN	$C_{\infty v}$	$^3\Sigma^-$	2.56	10.40	2.01
Si_2N	$D_{\infty h}$	$^1\Sigma_g^+$	5.13	11.53	
SiN_2[b]					
Si_3N	C_{2v}	$^1A_1$	4.79	8.38	
Si_2N_2	$D_{\infty h}$	$^2\Pi_g$	5.00	9.70	0.77
SiN_3	$C_{\infty v}$	$^1\Sigma$	5.64	18.78	
Si_4N	C_{3v}	$^1A_1$	4.63	8.25	
Si_3N_2	C_s	$^2A'$	5.45	10.26	0.76
Si_2N_3	C_s	$^3A''$	5.43	12.93	2.03
SiN_4	C_s	$^2A''$	5.30	11.44	0.87

[a] See footnote in Table 1

[b] No conformations were predicted

Table 4 Calculated vibrational frequencies (in cm^{-1}) at the HF/6-31G* level of the ground state structures. Symmetry and intensity are in parenthesis

Species	Frequencies
SiN	925 (σ, 30.2)
SiN^-	1322 (σ, 32.5)
SiN^+	814 (σ, 77.5)
Si_2N	214 (π_u, 9.4)[a], 291 (π_u, 20.1)[a], 623 (σ_g, 0.0), 821 (σ_u, 1773.8)
Si_2N^-	450 (a_1, 49.7), 746 (b_2, 6.1), 950 (a_1, 90.9)
Si_2N^+	237 (π_u, 27.6)[a], 237 (π_u, 27.6)[a], 695 (σ_g, 0.0), 1464 (π_u, 1230.6)
SiN_2	700 (a_1, 0.9), 845 (b_2, 13.9), 1693 (a_1, 158.7)
SiN_2^-	373 (π, 0.0)[a], 410 (σ, 286.7), 432 (π, 21.6)[a], 1870 (σ, 2980.9)
SiN_2^+	No structure was predicted
Si_3N	85 (a', 20.6), 282 (a'', 1.6), 349 (a', 25.1), 508 (a', 86.9), 674 (a', 70.0), 858 (a', 230.3).
Si_3N^-	11 (b_2, 13.2), 162 (b_1, 15.7), 168 (b_2, 0.9), 269 (a_1, 3.6), 593 (a_1, 0.1), 1297 (a_1, 0.2).
Si_3N^+	224 (π_u, 19.4) [a], 224 (π_u, 19.4) [a], 702 (σ_g, 0.0), 1473 (σ_u, 1243)
Si_2N_2	183 (π_u, 29.7)[a], 183 (π_u, 29.7)[a], 456 (π_g, 0.0)[a], 456 (π_g, 0.0)[a], 635 (σ_g, 0.0), 1349 (σ_g, 221.4), 1788 (σ_g, 0.0)
$Si_2N_2^-$	322 (B_1, 13.7), 511 (B_2, 0.0), 575 (A_1, 145.2), 650 (B_1, 0.0), 691 (B_2, 220.7), 934 (A_1, 0.0)
$Si_2N_2^+$	152 (π_u, 18.7)[a], 164 (π_u, 33.6)[a], 343 (π_g, 0.0)[a], 382 (π_u, 0.0)[a], 604 (σ_g, 0.0), 1099 (σ_g, 1126.5), 1925 (σ_g, 0.0)
SiN_3	192 (a', 13.7), 251 (a'', 15.3), 588 (a', 33.3), 818 (a', 8.0), 1341 (a', 1.9), 1528 (a', 70.2)
SiN_3^-	661 (e, 6.3), 661 (e, 6.3), 759 (a_1, 3.2), 909 (e, 26.4), 909 (e, 26.4), 1288 (a_1, 56.8)
SiN_3^+	168 (π, 18.6)[a], 168 (π, 18.6)[a], 635 (π, 31.8)[a], 635 (π, 31.8)[a], 755 (σ, 67.9), 1626 (σ, 948.5), 2714 (σ, 386.8)
Si_4N	90.4 (b_1, 1.1), 163 (b_2, 1.1), 262 (b_2, 1.9), 303 (b_1, 2.2), 386 (a_1, 0.8), 495 (a_1, 0.1), 529 (b_2, 22.6), 590 (a_1, 44.7), 1058 (a_1, 900.2)
Si_4N^-	273 (e, 10.6)[b], 273 (e, 10.6)[b], 340 (e, 16.2)[b], 340 (e, 16.2)[b], 459 (a_1, 0.7), 387 (a_1, 57.0), 541 (e, 2.3)[b], 541 (e, 2.3)[b], 799 (a_1, 87.1)
Si_4N^+	176 (e, 11.3) [b], 176 (e, 11.3) [b], 254 (e, 2.8) [b], 254 (e, 2.8) [b], 336 (a_1, 9.3), 422 (a_1, 62.5), 624 (e, 99.3) [b], 624 (e, 99.3) [b], 657 (a_1, 50.3)
Si_3N_2	25 (π, 1.2)[a], 25 (π, 12.6)[a], 158 (π, 12.6)[a], 158 (π, 12.6)[a], 262 (π, 17.4)[a], 262 (π, 17.4)[a], 470 (σ, 21.3), 882 (σ, 10.5), 1358 (σ, 137.0)
$Si_3N_2^-$	128 (b_1, 1.4), 161 (b_2, 2.2), 242 (b_1, 3.0), 446 (a_1, 1.4), 522 (b_2, 50.2), 551 (a_1, 58.5), 946 (a_1, 233.7), 992 (b_2, 432), 1138 (a_1, 467)
$Si_3N_2^+$	7.2 (a', 0.3), 21.4 (a', 1.1), 33.5 (a', 1.7), 74.8 (a', 1.7), 218 (a', 15.7), 241 (a', 25.1), 291 (a', 0.8), 715 (a', 8.7), 1463 (a', 1686)
Si_2N_3	123 (a', 9.9), 126 (a', 1.7), 340 (a', 6.8), 356 (a', 22.0), 564 (a', 11.0), 796 (a', 156.2), 982 (a', 271), 1065 (a', 257), 1518 (a', 248)
$Si_2N_3^-$	176 (b_1, 0.5), 322 (a_2, 0.0), 432 (b_1, 53.2), 491 (a_1, 17.1), 548 (a_1, 27.5), 723 (a_1, 6.0), 861 (a_1, 47.2), 1112 (b_2, 437), 1773 (a_1, 27.3)
$Si_2N_3^+$	86 (a', 1.1), 219 (a', 7.0), 234 (a', 14.4), 236 (a'', 34.4), 292 (a'', 0.4), 362 (a', 22.6), 701 (a', 3.0), 1460 (a', 761), 2418 (a', 228.3)
SiN_4	135 (a', 5.6), 313 (a'', 15.2), 370 (a', 20.1), 594 (a'', 17.4), 665 (a', 14.9), 936 (a', 9.2), 1217 (a', 280.5), 1641 (a', 1132.3), 2429 (a', 1132.3)
SiN_4^-	181 (b_1, 0.0), 257 (b_2, 2.1), 572 (a_1, 0.1), 837 (b_1, 0.0), 909 (b_2, 103.0), 1078 (a_1, 44.2), 1296 (b_2, 236.7), 1347 (a_1, 16.6), 1569 (a_1, 1.1)
SiN_4^+	65 (a'', 4.4), 168 (a', 26.1), 344 (a', 40.7), 452 (a'', 5.4), 685 (a', 32.2), 817 (a', 127.6), 1026 (a', 53.4), 1330 (a', 374), 2313 (a', 297)

[a] For the two Renner-Teller components of this Π electronic state

[b] For the two Jahn-Teller components of this doubly degenerate electronic state

of Kerkines and Mavridis [32] and the indirectly extracted experimental value of 1.604 Å, fall within the experimental error of present and previous calculations. For the SiN cation cluster, we computed an equilibrium distance in good agreement with that found by Goldberg et al. [44] [R_e (Si-N^+, $X^3\Sigma^-$)=1.78 Å)]. Similar conclusions can be drawn for the harmonic frequencies. See Table 4 for more details.

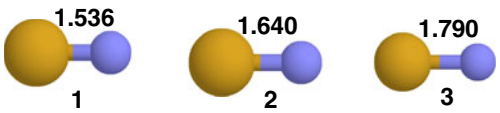

Fig. 1 Ground state structure of the SiN neutral (**1**), anion (**2**) and cation (**3**) clusters

Si_2N

The ground state predicted structure of the Si_2N neutral, anion and cation clusters is shown in Fig. 2. For the neutral Si_2N cluster, Goldberg et al. [44] showed that the inclusion of electron correlation stabilizes the linear form rather than

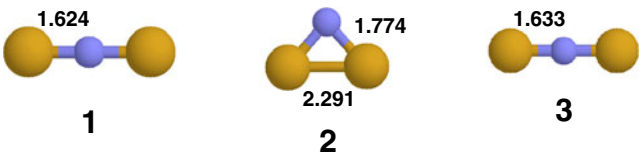

Fig. 2 Ground state structure of the Si_2N neutral (**1**), anion (**2**) and cation (**3**) clusters

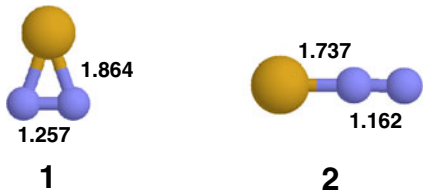

Fig. 3 Ground state structure of the SiN_2 neutral (**1**) and anion (**2**) clusters. No structure was predicted for the cation cluster, see text

the bent structure. At the G3 level, a bi-Si-terminated linear $D_{\infty h}$ structure is predicted for the neutral ($X^2\Pi_g$) and cation ($X^1\Sigma_g^+$) clusters, and a bent C_{2v} structure (X^1A_1) is predicted for the anion cluster. A similar bi-Si-terminated linear $D_{\infty h}$ structure to that of the neutral and cation clusters is predicted for the anion cluster only 0.06 eV, at the G3 level, higher in energy than that of the bent C_{2v} structure and of triplet state. For both the Si_2N anion and cation clusters, the ground state structure is singlet state. For the neutral species, we confirm the DFT results of Jungnickel et al. [46].

For the corresponding C_2N neutral and cation clusters, a similar singlet bi-C-terminated linear $D_{\infty h}$ structure is predicted to be the ground state. The predicted ground state structure of the C_2N anion cluster is a triplet C-terminated linear structure. The SiN bond length of the Si_2N neutral and cation clusters is predicted to be too close to each other, within less than 0.01 Å, with that of the cation cluster being longer. The SiN bond length of the Si_2N anion cluster is predicted to be about 0.15 Å longer than that of the Si_2N neutral cluster. For the C_2N neutral and cation clusters, the difference between the CN bond length of the neutral and cation clusters is also about 0.01 Å, with that of the cation cluster being longer, but that of the C_2N anion cluster is shorter than that of the neutral cluster by about 0.06 Å.

SiN_2

The ground state structure of the SiN_2 neutral and anion clusters is shown in Fig. 3. No stable structure was predicted for the cation cluster most likely because the potential energy surface is too flat so that the G3 methodology is not applicable. We have generated the three-dimensional (3D) potential energy surface (PES) of the SiN_2 cation cluster in the internal coordinates [R_1=R(SiN), R_2=R(NN), in-plane angle=θ] at the CASSCF/aug cc-pVTZ level of theory. The most stable isomer is a linear $X^2\Pi$ state SiNN cation cluster. The equilibrium geometry has a SiN bond length of 2.243 Å and NN bond length of 1.104 Å. The calculated harmonic frequencies at this level are 191 (bend), 206 (bend), 220 (stretch) and 2,334 (stretch) cm^{-1}. As can be seen in Fig. S30, the PESs are flat along the SiN elongation and the SiNN bending. This cannot be performed by the standard methodologies implemented in the Gaussian program.

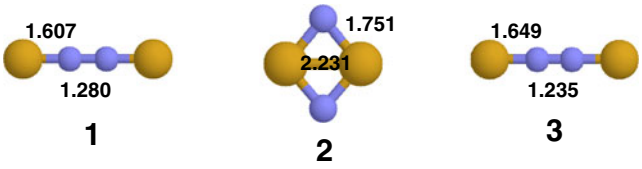

Fig. 5 Ground state structure of the Si_2N_2 neutral (**1**), anion (**2**) and cation (**3**) clusters

The predicted ground state structure of the SiN_2 neutral cluster is a singlet state triangular C_{2v} structure (X^1A_1) close to that found in [46]. The lowest predicted triplet state structure is higher in energy than the ground state singlet structure by 4.67 eV, at the G3 level. The predicted ground state structure of the SiN_2 anion cluster is a Si-terminated linear structure ($X^2\Pi$). A triangular C_{2v} structure similar to that of the SiN_2 neutral cluster is predicted for the SiN_2 anion cluster to be 0.86 eV higher in energy, at the G3 level. A Si-terminated linear structure similar to that of the SiN_2 anion cluster is predicted for the SiN_2 neutral cluster to be 0.44 eV higher in energy, at the G3 level, than the ground state triangular C_{2v} structure. Surprisingly, the SiN bond length of the SiN_2 neutral cluster is longer than that of the anion cluster by about 0.13 Å. This is contrary to that calculated for the SiN neutral and anion clusters. For the CN_2 cluster, a linear bi-N-terminated structure is predicted for both the neutral and anion clusters. This structure is predicted to be the highest energy predicted structure for the SiN_2 neutral and anion clusters with relative energies, at the G3 level, of 4.67 and 2.85 eV for the neutral and anion clusters, respectively.

Si_3N

Figure 4 depicts the predicted ground state structure of the Si_3N neutral (C_s, X^2A''), anion (C_{2v}, X^1A_1) and cation (C_{2v},

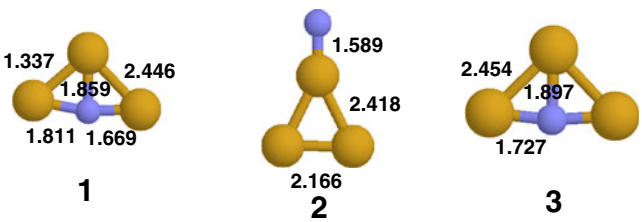

Fig. 4 Ground state structure of the Si_3N neutral (**1**), anion (**2**) and cation (**3**) clusters

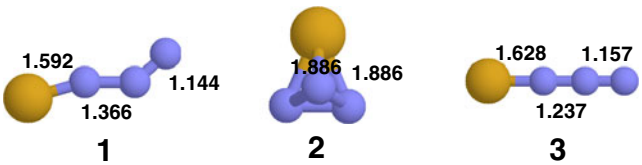

Fig. 6 Ground state structure of the SiN_3 neutral (**1**), anion (**2**) and cation (**3**) clusters

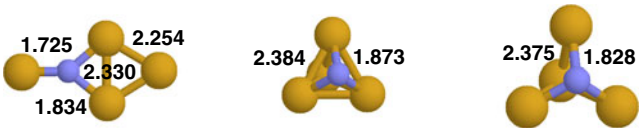

Fig. 7 Ground state structure of the Si_4N neutral (**1**), anion (**2**) and cation (**3**) clusters

X^1A_1) clusters. These structures are similar to those predicted at the MP2(full)/6-311+G* level treatment [44]. For the neutral and cation clusters a similar T-shaped structure is predicted with a C_s symmetry for the neutral cluster and a C_{2v} symmetry for the cation cluster. For the cation cluster, a similar C_{2v} structure of the neutral cluster has one imaginary vibrational frequency, while a similar C_s structure of triplet state for the cation cluster failed to converge at the HF level. A singlet state C_s structure of the cation cluster converged at the HF level to the same C_{2v} structure. The lowest energy predicted structure of the anion cluster is also a T-shaped Si-terminated structure. The second most stable structure of the neutral, anion and cation clusters is the same Si-terminated T-shaped structure, which lies higher in energy (but not more than 1.3 eV) at the G3 level, than the lowest energy predicted structure (Figs. S9–S11, Table S4). Both the anion and cation clusters have a triplet state. This structure for the three neutral, anion and cation clusters has similar bond lengths with a difference between the corresponding bond lengths of the three neutral, anion and cation clusters of less than only 0.03 Å. For the similar C_3N neutral, anion and cation clusters, a C-terminated linear structure was predicted as the ground state structure of the three clusters. For these three clusters, the elongation of the CN bond length is about 0.07 Å at the most upon addition or removal of an electron to the C_3N neutral cluster.

Si_2N_2

Here, a bi-Si-terminated linear structure is predicted to be the ground state structure of the Si_2N_2 neutral and cation clusters. For the neutral Si_2N_2 cluster, DFT also leads to a similar structure [46]. For the Si_2N_2 anion cluster, a square structure is predicted to be the ground state structure. For the similar C_2N_2 neutral and cation clusters, a linear structure is also predicted to be the ground state structure but in this case it is bi-N-terminated, rather than bi-Si-terminated. The C_2N_2 anion cluster is predicted to have a zigzag, also bi-N-terminated, structure as the ground state structure [54]. The predicated

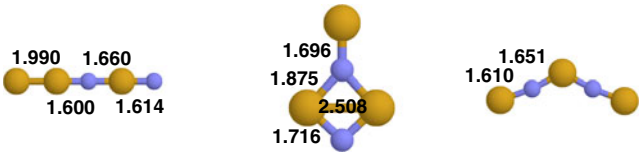

Fig. 8 Ground state structure of the Si_3N_2 neutral (**1**), anion (**2**) and cation (**3**) clusters

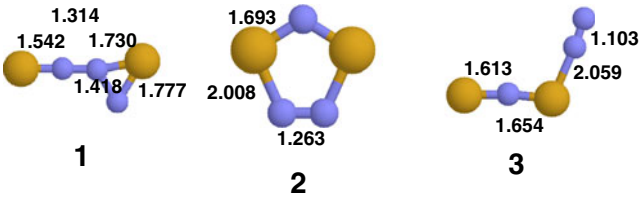

Fig. 9 Ground state structure of the Si_2N_3 neutral (**1**), anion (**2**) and cation (**3**) clusters

ground state structure of the Si_2N_2 neutral cluster is singlet state ($X^1\Sigma_g^+$). The lowest energy triplet state predicated structure of the Si_2N_2 neutral cluster is structure **7** (Table S5, Fig. S12), which has an L-shaped structure that is higher in energy by 1.86 eV, according to the G3 level, than the ground state structure. While ten structures were predicted for the Si_2N_2 neutral cluster, only three and two structures were predicted for the Si_2N_2 anion and cation clusters, respectively. None of the predicted structures of the Si_2N_2 cluster is a bi-N-terminated linear structure (Figs. S12–S14). Similar to the Si_3N cluster, for the ground state Si_2N_2 neutral and cation clusters, there is no significant difference between the SiN and NN bond lengths, within about 0.05 Å, of the neutral and cation clusters. However, the SiN bond length of the Si_2N_2 anion cluster is longer by about 0.14 Å.

SiN_3

Only two structures were predicted for the SiN_3 neutral cluster: one is a Si-terminated zigzag structure and the second is a Si-terminated T-shaped structure. The latter structure is higher in energy than the ground state structure (X^2A'), at the G3 level, by 2.83 eV. The predicted ground state structure of the SiN_3 cation cluster ($X^1\Sigma^+$) is a Si-terminated linear structure, while a tetrahedral structure was predicted as the ground state structure of the SiN_3 anion cluster (X^1A_1). For the analogous CN_3 neutral, anion and cation clusters, a N-terminated T-shaped, bi-N-terminated V-shaped, and bi-N-terminated linear structures, respectively, were predicted as the ground state structures. The ground states of the SiN_3 anion and cation clusters are singlet. The energy difference between the ground state singlet structure and the first lowest energy triplet state structure at the G3 level is 0.25 and 4.08 eV for the anion and cation clusters,

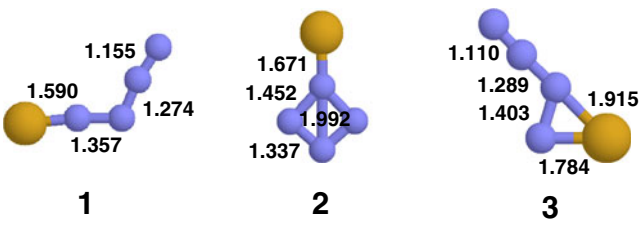

Fig. 10 Ground state structure of the SiN_4 neutral (**1**), anion (**2**) and cation (**3**) clusters

respectively. Assuming the neutral and cation clusters have a somewhat similar structure, as was mentioned above for the other silicon-nitrogen clusters, there is a small difference between the bond lengths of the neutral and cation clusters, within 0.04 Å, with that of the cation cluster being longer than that of the neutral cluster. An exception is the central N–N bond where the difference is 0.13 Å, with that of the cation cluster being shorter than that of the neutral cluster.

Si_4N

The Si_4N cluster has the largest number of Si atoms of the clusters considered in this work. The ground state predicted structures of the Si_4N neutral (X^2B_2), anion (X^1A_1) and cation (X^1A_1) clusters are an Si-terminated rhombic structure with an external Si atom connected to the unique nitrogen atom, triagonal bipyramidal and triagonal bipyramidal structures, respectively (Fig. 7). For the neutral and cation clusters, none of the predicted structures are linear (Figs. S18, S20). Hence we confirm the 3D structure found by DFT [46] for the anion and the cation clusters whereas we compute a planar structure for the neutral cluster. For the anion cluster, a linear structure is predicted, structure **12** (Fig. S19), which is 3.24 eV higher in energy at the G3 level than the ground state structure (Table S12). The ground state structure of the anion and cation clusters is singlet. For the anion cluster, the lowest energy triplet state structure is structure **4**, which is also of triagonal bipyramidal structure and higher in energy by 1.02 eV at the G3 level than the ground state singlet structure. For the cation structure, a T-shaped structure (structure **5** in Table S19 and Fig. S20) is the lowest energy triplet state structure, which is higher in energy by 0.77 eV at the G3 level than the ground state singlet structure. The corresponding C_4N neutral, anion and cation clusters have bi-N-terminated V-shaped, pentagonal and bi-N-terminated V-shaped structures, respectively. The SiN and SiSi bond lengths of the triagonal bipyramidal structures of the anion and cation clusters (Fig. 7), are close to each other within 0.05 Å at most, with that of the anion cluster longer than that of the cation cluster for both the Si–N and Si–Si bonds.

Si_3N_2

This cluster is characterized by the large number of predicted clusters: 17, 17 and 9, for the Si_3N_2 neutral, anion and cation clusters, respectively. An alternate SiN singlet state linear structure is predicted as the ground state structure for the Si_2N_3 neutral cluster—a reflection of the stability of the SiN bond over the Si–Si and N–N bonds. The lowest energy triplet state structure (structure **5**, Fig. S21, Table S14) is a pyramidal structure that is higher in energy than the ground state singlet structure at the G3 level by 3.64 eV. The predicted ground state structures of the anion and cation clusters are Si-terminated T-shaped and bi-Si-terminated V-shaped structures, respectively. Interestingly, the SiN bond lengths of the Si_2N_3 neutral, anion and cation clusters are comparable to those of the corresponding SiN neutral, anion and cation clusters, within 0.08 Å, with that of the Si_2N_3 clusters being longer. The predicted structures of the corresponding C_2N_3 neutral, anion and cation clusters are bi-N-terminated linear, V-shaped and T-shaped structures, respectively.

Si_2N_3

This cluster has the largest number of predicted structures: 7, 26 and 16 for the neutral, anion and cation clusters (Figs. S24–S26), respectively, in this work. A Si-terminated T-shaped-like structure is predicted as the ground state structure (X^2A'') of the Si_2N_3 neutral cluster (Fig. 9). This differs from the DFT results. This is not surprising for this large number of isomers, the order of which should depend strongly on the electron correlation accounted for. Indeed, the high density of structures is associated with a high density of electronic states of different spin-multiplicities close to the ground state, which are not described equivalently by the DFT or ab initio approaches. This is the case, for instance, for pure carbon chains (C_n) or their hydrides (HC_n) [55–61].

Only one linear structure is predicted for this Si_2N_3 neutral cluster (structure **6**, Fig. S24). This linear structure is predicted to be higher in energy by 1.26 eV at the G3 level than the ground state structure. The ground state structures of the Si_2N_3 anion and cation clusters are of singlet state pentagonal (X^1A_1) and triplet state V-shaped (X^3A'') nature, respectively (Fig. 9). For the corresponding C_2N_3 neutral, anion and cation clusters, bi-C-terminated V-shaped, V-shaped and linear structures, respectively, are predicted as the ground state structures. It might be constructive at this point to compare the SiN bond length of the SiN neutral, anion and cation clusters and those of the corresponding Si_2N_3 neutral, anion and cation clusters. The calculated SiN bond lengths of the SiN neutral, anion and cation clusters at the MP2/6-31G* level are 1.536, 1.640 and 1.790 Å, respectively (Fig. 1). At the same MP2/6-31G* level, the calculated SiN bond lengths for the Si_2N_3 neutral, anion and cation clusters are 1.542 Å (for the terminal SiN bond), 1.693 Å (for one of the SiN bonds and 2.008 Å for the other bond) and 1.613 Å (for the terminal SiN bond), respectively (Fig. 9). It is interesting to note then that there is no significant change in the SiN bond lengths (within 0.06 Å) for the corresponding neutral and anion clusters, with those of the SiN clusters being shorter than those of the corresponding Si_2N_3 clusters. However, for the cation clusters the difference is as much as about 0.18 Å, with that of the SiN cluster longer than that of the Si_2N_3 cluster. It is clear from the SiN bond

lengths of the Si_2N_3 neutral, anion and cation clusters, mentioned above, that there is an elongation of SiN bond length upon addition or removal of an electron.

SiN_4

The ground state predicted structure of the SiN_4 neutral cluster is singlet state Si-terminated V-shaped structure (Fig. 10). In fact, the three lowest energy structures of the SiN_4 neutral cluster are V-shaped or V-shaped-like structures (Fig. S27). No linear structure was predicted for this SiN_4 neutral cluster. The lowest energy triplet state structure is less stable than the ground state structure by only 0.64 eV at the G3 level (Table S20). This triplet state structure has a pyramidal structure (structure **4**, Fig. S27). The ground state predicted structure of the SiN_4 anion cluster is a Si-terminated structure, while that of the SiN_4 cation cluster is a N-terminated structure. For the SiN_4 anion and cation clusters, similar to the SiN_4 neutral cluster, no linear structure was predicted (Figs. S28, S29). Both the predicted structures of the Si_4N anion and cation structures have T-shaped-like structures. For the similar CN_4 neutral, anion and cation clusters, the predicted ground state structures had V-shaped, pentagonal and V-shaped structures, respectively. Neither of the V-shaped structure of the CN_4 neutral and cation clusters is an N-terminated structure. The calculated SiN bond length of the SiN_4 neutral, anion and cation clusters is 1.590, 1.671 and 1.915/1.784 Å, respectively. There is then a significant elongation, within 0.3 Å, of the SiN bond length upon addition or removal of an electron.

Binding energy, HOMO-LUMO gap, vertical electron attachment, adiabatic electron affinity, and vertical ionization energy

Tables 1–3 list the calculated BE, HLG, VEA, AEA and VIE at the G3 level of the ground state structure of the SiN, Si_2N, SiN_2, Si_3N, Si_2N_2, SiN_3, Si_4N, Si_3N_2, Si_2N_3 and SiN_4 clusters in the neutral, anion (BE and HLG only) and cation (BE and HLG only) forms. The calculated BE, HLG, VEA, AEA and VIE at the G3 level of all predicted structures of all considered clusters in the current work are listed in Tables S1–S22. The VEA, AEA and VIE are calculated for the neutral clusters only. Figure 11 represents the variation in the BE, for the neutral, anion and cation clusters, as the cluster size increases due to the increase in the number of Si atoms. Figure 12 represents the variation in BE, for the neutral, anion and cation clusters, as the cluster size increases due to the increase in the number of N atoms. Figure 13 represents the variation in BE, of the neutral, anion and cation clusters for the five-atom clusters with the increase of the number of N atoms and consequent decrease of the

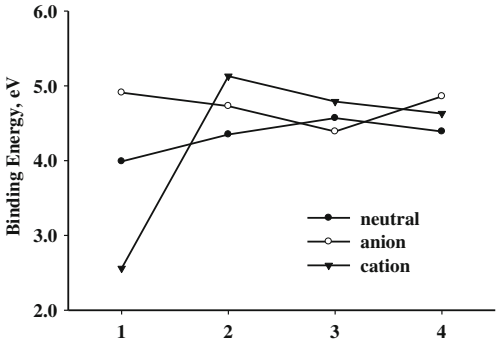

Fig. 11 Calculated binding energy (BE, eV) at the G3 level of the SiN (1), Si_2N (2), Si_3N (3) and Si_4N (4) clusters

number of Si atoms. Figures 14, 15 and 16 are similar to Figs. 11, 12 and 13 except that they are for the HLG. Figures 17, 18 and 19 represent the variations as those in Figs. 11, 12 and 13 except they are for the VEA, AEA and VIE of the neutral clusters. The data in Figs. 12 and 15 show a discontinuation of the lines corresponding to the SiN_2 cation cluster since we were not able to identify stable structures of the SiN_2 cation cluster.

Binding energy

The calculated BEs of all considered clusters, except that of the SiN cation cluster, fall in the range of 4–6 eV. The calculated BEs of the similar C_nN_m clusters fall in the range of 5–7 eV. This reflects the higher stability of C_nN_m clusters over Si_nN_m clusters. The calculated BE of the SiN cation cluster has the lowest value of all clusters considered in this work, of only 2.56 eV (Table 3). The data in Fig. 11 reflects a general decrease of the stability of the Si_nN_m clusters with the increase of the number of the Si atoms, whereas the data in Fig. 12 reflect the increase in the stability of the clusters by the increase in the number of nitrogen atoms. The results displayed in Fig. 13 generally support this conclusion as the

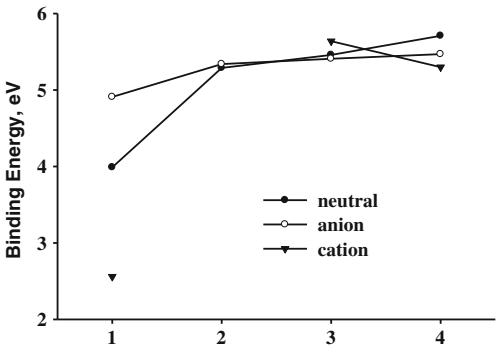

Fig. 12 Calculated BE (eV) at the G3 level of the SiN (1), SiN_2 (2), SiN_3 (3) and SiN_4 (4) clusters

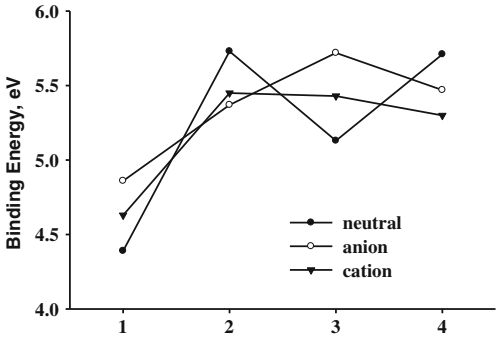

Fig. 13 Calculated BE (eV) at the G3 level of the Si_4N (1), Si_3N_2 (2), Si_2N_3 (3) and SiN_4 (4) clusters

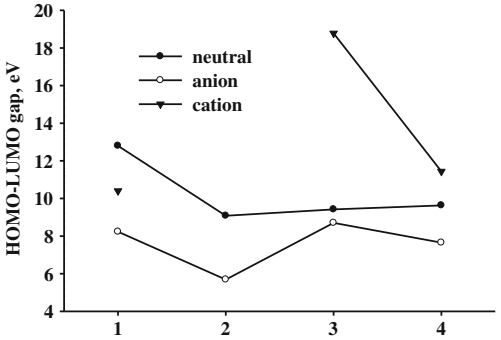

Fig. 15 HLG (eV) at the G3 level of the SiN (1), SiN_2 (2), SiN_3 (3) and SiN_4 (4) clusters

Si_4N, neutral, anion and cation, clusters have the lowest BE and the SiN_4, neutral, anion and cation, clusters have almost the highest BE. A similar conclusion was drawn about the similar C_nN_m clusters, where there was an increase in the BE with the increase in the number of N atoms and consequent decrease in the number of C atoms.

HOMO-LUMO gap

Compared to the similar C_nN_m clusters, the Si_nN_m clusters considered in this work have a generally lower HLG, while the odd-even rule is also not clear cut for either the Si_nN_m or C_nN_m clusters. For example, the HLG of most of the Si_nN_m clusters falls in the range of 6–14 eV, while that of the C_nN_m clusters falls in the range of 9–16. As already noted from the calculated BEs, this reflects the higher stability of the C_nN_m clusters over the Si_nN_m clusters. It is also interesting to note, similar to the C_nN_m clusters, that the cation clusters have generally the highest HLG, reflecting their higher stability over the neutral and anion clusters. The SiN_3 cation cluster has the highest HLG (18.78 eV, Table 3) of all clusters considered in this work. In fact this cluster has one of the highest BEs of all of the clusters considered in this work.

Vertical electron attachment, adiabatic electron affinity, and vertical ionization energy

It is interesting here to compare between the VEA, AEA and VIE of the Si_nN_m and C_nN_m, m=1–4, n=1–4, $m+n$=2–5, clusters. Indeed, it is interesting to note that the VEA, AEA and VIE of all the C_nN_m clusters are higher than those of the corresponding Si_nN_m clusters. The only exception is the VEA of the Si_3N_2 cluster and the AEA of the Si_2N_2, Si_3N_2 and Si_4N clusters. As mentioned with the BE and HLG, this is due to the higher stability of the C_nN_m clusters over the similar Si_nN_m clusters. As shown in Fig. 19 and Table 1, the Si_3N_2 cluster has the highest VIE and AEA, while the VIE of the same Si_3N_2 cluster has the lowest VIE, indicating that it is the most stable of the Si_nN_m clusters considered in this work.

General tendencies

Bent structures became more stable as $m+n$ increases for the neutrals, anionic and cationic clusters, which is also the case for their carbon–nitrogen counterparts. For C_nN_m clusters with $m+n$=2–5, most of the predicted lowest energy structures of the clusters were linear. For the Si_nN_m clusters with $m+n$=2–5 neural and cationic clusters, the situation is less obvious since N-rich clusters lead mostly to linear or

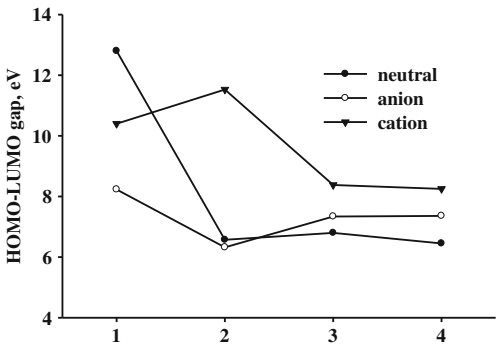

Fig. 14 HLG (eV) at the G3 level of the SiN (1), Si_2N (2), Si_3N (3) and Si_4N (4) clusters

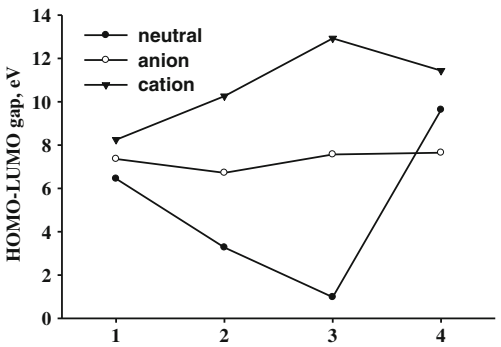

Fig. 16 HLG (eV) at the G3 level of the Si_4N (1), Si_3N_2 (2), Si_2N_3 (3) and SiN_4 (4) clusters

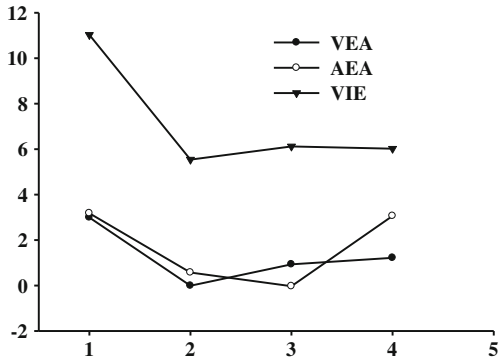

Fig. 17 Vertical electron attachment (VEA), adiabatic electron affinity (AEA) and vertical ionization energy (VIE, eV) at the G3 level of the SiN (1), Si_2N (2), Si_3N (3) and Si_4N (4) clusters

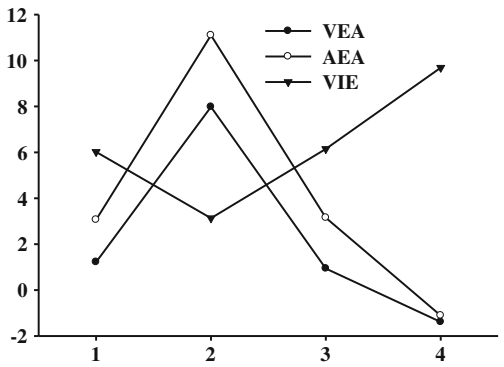

Fig. 19 VEA, AEA and VIE (eV) at the G3 level of the Si_4N (1), Si_3N_2 (2), Si_2N_3 (3) and SiN_4 (4) clusters

quasilinear conformers and Si-rich clusters favor planar or 3D structures as already noted in [46]. For Si_nN_m anionic species, the $m+n$ increase favors 3D structures, whereas their corresponding C_nN_m clusters are also mostly linear. Such structural differences due to the carbon/silicon substitution are not surprising since it is also observable for common organic compounds. For instance, acetylene HCCH is linear whereas Si_2H_2 is a 3D di-bridged or 'butterfly'-like molecule [62].

Strictly speaking, the number of clusters studied here is not large enough to derive major solid tendencies for BE, HLG, VEA, AEA or VIE. However, a few important remarks can be made about the stability and behavior of these clusters. The higher the value of BE, the more stable the cluster. For the corresponding C_nN_m clusters, the values of the BE of these clusters are in the range of 5–7 eV. For the Si_nN_m clusters considered in the current study the values of the BE are in the range of 4–6 eV. This confirms the higher stability of carbon–nitrogen clusters over silicon–nitrogen clusters. The SiN neutral and cation clusters have the lowest BE. That of the SiN neutral cluster has the lowest BE of only 2.56 eV (Table 3) for all clusters considered in this work. Moreover, it is interesting to note from Fig. 13 that, for five-atoms clusters, the Si_4N neutral, anion and cation clusters have the lowest BE. This was noted also for the corresponding C_nN_m clusters, where there was an increase in BE with the increase in the number of the nitrogen atoms and consequent decrease in the number of carbon atoms. Otherwise, due to the limited number of clusters considered in the current study it is not possible to derive more general conclusions.

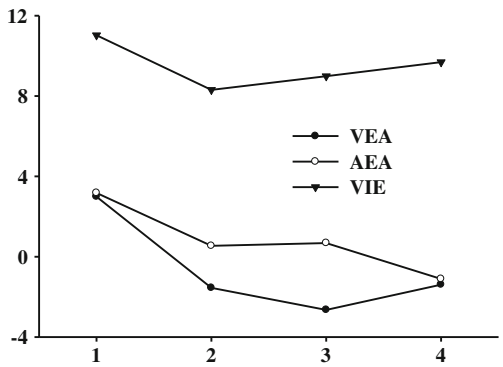

Fig. 18 VEA, AEA and VIE (eV) at the G3 level of the SiN (1), SiN_2 (2), SiN_3 (3) and SiN_4 (4) clusters

Conclusions

We presented a detailed theoretical characterization of the most stable isomers of the neutral, anionic and cationic Si_nN_m clusters. This allows knowledge of their relative stability, of their structural and thermochemical and spectroscopic properties to be expanded. This is certainly an important step for the determination of their composition and the possible reactions leading to their formation in both laboratory and industrial environments, reactions that occur either in the gas phase, on small aggregates or on silicon surfaces. The results of the present systematic study should be useful in modeling and understanding the growth of silicon-based clusters at the nano scale. Our work should also motivate new experimental studies on this important class of clusters. Their complete identification and characterization is mandatory to improving use of their potentialities in fundamental and applied areas.

Acknowledgments Supported by NPST program by King Saud University Project Number: ADV400-02. M.H. thanks the PCMI program (INSU, CNRS, FRANCE) for financial support.

References

1. Al-Mogren MM, El-Azhary AA, Alkiali WZ, Hochlaf M (2010) J Phys Chem A 114:12258–12264
2. Turner BE (1991) Bull Am Astron Soc 23:933–938
3. Turner BE (1992) ApJ 388:L35–L38

4. Hughes DW (1978) In: McDonnell JAM (ed) Cosmic dust. Wiley, Chichester
5. Plane JMC (2003) Chem Rev 103:4963–4984
6. Koeberl C, Hagen EH (1989) Geochim Cosmochim Acta 53:937–944
7. Vondrak T, Plane JMC, Broadley S, Janches D (2008) Atmos Chem Phys Discuss 8:14557–14606
8. Gómez Martín JC, Blitz MA, Plane JMC (2009) Phys Chem Chem Phys 11:671–678
9. Ferguson EE, Fahey DW, Fehsenfeld FC, Albritton DL (1981) Planet Space Sci 29:307–312
10. Brown GA, Robinette WC Jr, Carlson HG (1968) J Electrochem Soc 115:948–955
11. Burns GT, Chandra G (1989) J Am Ceramic Soc 72:333–337
12. Riley FL (2000) J Am Ceramic Soc 83:245–265
13. Zhu W, Neumayer D, Perebeinos V, Avouris P (2010) Nano Lett 10:3572–3576
14. Zhang DY, Pouchan C, Jacquemin D, Perpète EA (2005) Chem Phys Lett 408:226–231
15. Bozso F, Avouris P (1986) Phys Rev Lett 57:1185–1188
16. Ray U, Jarrold MF (1990) J Chem Phys 93:5709–5719
17. Wlodek S, Bohme DK (1988) J Am Chem Soc 110:2396–2399
18. Low MJD, Ramasubramanian N, Subba Rao VV (1967) J Phys Chem 71:1726–1734
19. Parisel O, Hanus M, Ellinger Y (1996) Chem Phys 212:331–351
20. Chen HL, Wu CW, Ho JJ (2006) J Phys Chem A 110:8893–8900
21. Chen W-K, Lu I-C, Chaudhuri C, Huang W-J, Lee S-H (2008) J Phys Chem A 112:8479–8486
22. Hochlaf M, Chambaud G, Senent ML (2010) Mol Phys 108:1277–1284
23. Lauvergnat D, Senent ML, Jutier L, Hochlaf M (2011) J Chem Phys 135:074301–074309
24. Elhanine M, Hanoune B, Guelachvili G, Amiot C (1992) J Phys (Fr) 2:931–938
25. Ito H, Suzuki K, Kondow T, Kushitsu K (1993) Chem Phys Lett 208:328–334
26. Naulin C, Costes M, Moudden Z, Ghanem N, Dorthe G (1993) Chem Phys Lett 202:452–458
27. Bruna PJ, Dohmann H, Peyerimhoff S (1984) Can J Phys 62:1508–1523
28. Chong DP (1994) Chem Phys Lett 220:102–108
29. Cai Z-L, Martin JML, François JP, Gijbels R (1996) Chem Phys Lett 252:398–404
30. Borin AC (1996) Chem Phys Lett 262:80–86
31. Jursic BS (1998) J Mol Struct (THEOCHEM) 455:77–83
32. Kerkines ISK, Mavridis AJ (2005) Chem Phys 123:124301–124306
33. Meloni G, Sheehan SM, Ferguson MJ, Neumark DMJ (2004) Phys Chem A 108:9750–9754
34. Lembke RR, Ferrante RF, Weltner W Jr (1977) J Am Chem Soc 99:416–423
35. Iraqi M, Goldberg N, Schwarz H (1993) J Phys Chem 97:11371–11372
36. DeKock RL, Grev RS, Schaefer HF (1988) J Chem Phys 89:3016–3027
37. Ignatyev IS, Schaefer HF (1992) J Phys Chem 96:7632–7634
38. Cai ZL, Wang YF, Xiao HM (1992) J Chem Soc Faraday Trans 88:1611–1613
39. Dixon DA, DeKock RL (1992) J Chem Phys 97:1157–1161
40. Murray CW, Laming GJ, Handy NC, Amos RD (1993) J Phys Chem 97:1868–1871
41. Wang J, Erikson LA, Boyd RJ, Shi Z, Johnson BG (1994) J Phys Chem 98:1844–1850
42. Ornellas FR, Ueno LT, Iwata S (1997) J Chem Phys 106:151–157
43. Ornellas FR, Iwata S (1996) J Phys Chem 100:10919–10927
44. Goldberg N, Iraqi M, Schwarz H, Boldyrev A, Simons J (1994) J Chem Phys 101:2871–2879
45. Jackson KA, Jungnickel G, Frauenheim T (1998) Chem Phys Lett 292:235–242
46. Jungnickel G, Frauenheim T, Jackson KA (2000) J Chem Phys 112:1295–1305
47. Ornellas FR, Iwata S (1996) J Phys Chem 100:16155–16161
48. Ueno LT, Ornellas FRJ (2001) Braz Chem Soc 12:99–108
49. Li B-X, Wang G-Y, Ding W-F, Ren X-J, Ye J-Z (2009) Physica B 404:1679–1685
50. Frisch MJ, Trucks GW, Schlegel HB, Scuseria GE, Robb MA, Cheeseman JR, Scalmani G, Barone V, Mennucci B, Petersson GA et al (2009) Gaussian 03 and Gaussian 09, Revision A.1, Gaussian, Wallingford CT
51. Curtiss LA, Raghavachari K, Redfern PC, Rassolov V, Pople JA (1998) Gaussian-3 (G3) theory for molecules containing first and second-row atoms. J Chem Phys 109:7764–7776
52. Larry A. Curtiss1,Krishnan Raghavachari, Theor Chem Acc (2002) 108:61–70
53. Saito S, Endo Y, Hirota E (1983) J Chem Phys 78:6447–6450
54. Nsangou M, Senent ML, Hochlaf M (2009) Chem Phys 355:164–168
55. Jochnowitz EB, Maier JP (2008) Annu Rev Phys Chem 59:519–544
56. Massó H, Senent ML, Rosmus P, Hochlaf M (2006) J Chem Phys 124:234304–234308
57. Senent ML, Massó H, Hochlaf M (2007) Astrophys J 670:1510–1517
58. Massó H, Veryazov V, Malmqvist P-Å, Roos BO, Senent ML (2007) J Chem Phys 127:154318–154319
59. Massó H, Senent ML (2009) J Phys Chem A 113:12404–12410
60. Senent ML, Hochlaf M (2010) Astrophys J 708:1452–1458
61. Hammoutene D, Hochlaf M, Senent ML (2012) Mon Not R Astron Soc 424:1224–1231
62. Bogey M, Bolvin H, Demuynck C, Destombes J-L (1991) Phys Rev Lett 66:413–416